Cent. Eur. J. Geosci. • 4(2) • 2012 • 275-286
DOI: 10.2478/s13533-011-0053-z

VERSITA

Central European Journal of **Geosciences**

Quartz precipitation and fluid inclusion characteristics in sub-seafloor hydrothermal systems associated with volcanogenic massive sulfide deposits

Research Article

Matthew Steele-MacInnis*, Liang Han, Robert P. Lowell, J. Donald Rimstidt, Robert J. Bodnar

Department of Geosciences, Virginia Tech,
4044 Derring Hall, Blacksburg, VA 24061 USA

Received 20 October 2011; accepted 30 January 2012

Abstract: Results of a numerical modeling study of quartz dissolution and precipitation in a sub-seafloor hydrothermal system have been used to predict where in the system quartz could be deposited and potentially trap fluid inclusions. The spatial distribution of zones of quartz dissolution and precipitation is complex, owing to the fact that quartz solubility depends on many inter-related factors, including temperature, fluid salinity and fluid immiscibility, and is further complicated by the fact that quartz exhibits both prograde and retrograde solubility behavior, depending on the fluid temperature and salinity. Using the *PVTX* properties of H_2O-NaCl, the petrographic and microthermometric properties of fluid inclusions trapped at various locations within the hydrothermal system have been predicted. Vapor-rich inclusions are trapped as a result of the retrograde temperature-dependence of quartz solubility as the convecting fluid is heated in the vicinity of the magmatic heat source. Coexisting liquid-rich and vapor-rich inclusions are also trapped in this region when quartz precipitates as a result of fluid immiscibility that lowers the overall bulk quartz solubility in the system. Fluid inclusions trapped in the shallow subsurface near the seafloor vents and in the underlying stockwork are liquid-rich with homogenization temperatures of 200-400°C and salinities close to that of seawater. Volcanogenic massive sulfide (VMS) deposits represent the uplifted and partially eroded remnants of fossil submarine hydrothermal systems, and the relationship between fluid-inclusion properties and location within the hydrothermal system described here can be used in exploration for VMS deposits to infer the direction towards potential massive sulfide ore.

Keywords: seafloor hydrothermal systems • volcanogenic massive sulfide deposits • silica • quartz veins • fluid inclusions

*E-mail: mjmaci@vt.edu

1. Introduction

1.1. Fluid inclusions in submarine hydrothermal systems and volcanogenic massive sulfide deposits

Volcanogenic massive sulfide (VMS) deposits represent the fossil analogues of the active seafloor hydrothermal systems that are found at oceanic spreading centers [1]. Fluid inclusion (FI) studies of both active ("black smokers"; e.g. [2–4]) and fossil (e.g., [5, 6]) VMS systems have provided much information on the physical and chemical conditions of formation of these deposits. The characteristics of fluid inclusions in these systems, including room temperature phase ratios and microthermometric properties, are related to the *PVTX* conditions at which the FI formed, which in turn are related to the location within the hydrothermal system where the FI were trapped. For example, the properties of FI in samples from the JADE field in the Central Okinawa Trough, Japan, vary systematically with sampling location and position within the paragenesis, with evidence of phase separation in the deeper stockwork zone and mixing of hydrothermal fluids with seawater associated with the shallower stockworks, mounds and chimneys [3].

In active systems, samples for FI study include seafloor dredge and submersible vehicle grab samples (e.g., [3]), or samples obtained by submarine drilling (e.g., [2, 4]). Samples obtained from the seafloor by dredging or vehicle grab represent material formed at or very near the seafloor and typically do not contain quartz, and FI studied from these samples are mostly hosted in sulfide or sulfate minerals, especially sphalerite, barite and anhydrite [2, 3]. Although quartz is mostly absent from the seafloor mounds at active vents [7], quartz is a common mineral in samples from beneath the seafloor (obtained by drilling) and in the stockwork zones of VMS deposits [1, 4]. The stockwork zones that develop beneath active hydrothermal vents, and quartz that precipitates in those regions, have been mostly observed and studied in VMS deposits that represent fossil submarine hydrothermal systems that have been uplifted and partially eroded – these zones are rarely exposed in the modern seafloor [3].

In VMS deposits where quartz-bearing stockwork mineralization is present, quartz is one of the main host minerals for FI (see, for example, Table 4 of [8]). Primary inclusions in quartz are trapped as quartz precipitates from hydrothermal fluid [9] – it is unlikely that primary inclusions would be trapped when quartz is being dissolved. Note, however, that secondary fluid inclusions, which form during crack healing, may form as a result of localized dissolution-re-precipitation reactions taking place at *PTX* conditions at which quartz is mostly being dissolved. Therefore, *PTX* conditions during episodes of quartz dissolution are likely to be under-represented in the primary inclusion record, although those conditions may be preserved in secondary inclusions, or in primary inclusions in other host phases that are forming contemporaneously. The properties of quartz-hosted FI can provide information on the physical and chemical conditions of quartz precipitation and, if the quartz is forming in equilibrium with sulfides, these conditions also represent the conditions of sulfide mineralization.

The occurrence of phase separation in sub-seafloor hydrothermal systems is now widely recognized based on vent chemistry data (e.g., [10]). Fluid inclusion assemblages in quartz from active and recent VMS-forming submarine hydrothermal systems sometimes contain coexisting liquid-rich and vapor-rich inclusions, indicating that the host quartz was precipitated from immiscible fluids ([8], and references therein). Halite-bearing inclusions are generally not associated with mineralization in VMS deposits, but they do occur in the deeper parts of the system, below VMS mineralization. These deep, high-salinity FI may represent brine generated during phase separation, although the inclusions commonly do not show unequivocal petrographic evidence of phase separation. For example, fluid inclusion assemblages hosted in sphalerite from the JADE hydrothermal field in the Central Okinawa Trough, Japan contain high-salinity (albeit halite-absent) fluid inclusions, but do not have coexisting vapor-rich inclusions [3]. Fluid inclusion assemblages showing direct evidence of fluid phase immiscibility (coexisting vapor-rich and halite-bearing inclusions in the same fluid inclusion assemblage) have been observed in anhydrite from active vent sites at the PACMANUS field [2]. Similarly, petrographic evidence of immiscibility has been observed in quartz-hosted fluid inclusion assemblages from the Semail ophiolite (Oman) [11].

In the present study, we couple numerical fluid flow modeling of a sub-seafloor hydrothermal system with a model for dissolution and precipitation of quartz as a function of temperature, pressure and fluid salinity. Importantly, the fluid flow model accommodates two-phase (liquid + vapor) flow using the *PVTX* and thermodynamic properties of the system H_2O-NaCl as an analog for seawater. Results of the fluid flow and quartz transport model are then applied to predict where in the hydrothermal system quartz is likely to precipitate and trap FI, and the mechanisms responsible for quartz precipitation. We then use the *PVTX* properties of H_2O-NaCl fluids to predict the room temperature characteristics and microthermometric behavior of fluid inclusions trapped at specific locations within an active sub-seafloor hydrothermal system. We

relate these results to fluid inclusions observed in VMS deposits, and discuss how the spatial distribution of fluid inclusion types can be applied in exploration by providing vectors to guide the explorationist toward VMS-type mineralization. We emphasize that the results presented here are specifically applicable to fluid inclusions in quartz. However, as described above, quartz is usually not found in association with seafloor vents and mounds [7]. For completion, we describe the types of fluid inclusions that might be trapped in quartz in these near-seafloor features, even though quartz is unlikely to be found in these environments. At the shallowest levels of the submarine hydrothermal system near the seafloor, FI with the characteristics described here are, however, likely to be found in phases that are common in this environment, such as sphalerite, barite and anhydrite. In the present study, we focus on the properties of FI hosted in quartz in the deeper regions, below the seafloor mounds.

1.2. Relationships between fluid phase equilibria, fluid inclusion characteristics and quartz solubility

Figure 1 shows the phase equilibria as a function of temperature and pressure for an H_2O-NaCl solution containing 3.2 mass% NaCl, representing the composition of seawater. The phase behavior shown in Fig. 1 is based on the model of [12]. Also shown on Figure 1 are quartz solubility isopleths (labeled in mmolal SiO_2), determined using the model of [13]. The liquid-vapor curve (the thick solid curve in Fig. 1) separates the single-phase fluid field (blue = liquid, yellow = vapor, Fig. 1) from the liquid + vapor field (green, Fig. 1). The critical isochore (dashed line, Fig. 1) divides the single-phase fluid field into the fields of liquid (to the left of the critical isochore) and vapor (to the right of the critical isochore).

Fluid inclusions trapped at *PT* conditions within the liquid field in Fig. 1 have a density greater than the critical density for this composition (0.443 g/cm^3; [14]). These inclusions contain liquid and a vapor bubble occupying $\leq$ 60 volume percent of the inclusion at room temperature, and homogenize to the liquid phase by shrinkage and disappearance of the vapor bubble at the homogenization temperature (e.g., the inclusion trapped at point "2" in Fig. 1). Inclusions trapped in the lower temperature range in Fig. 1 may remain metastable and not nucleate a bubble when cooled [9, 15], and therefore contain only liquid at ambient laboratory conditions (e.g., the inclusion trapped at point "1" in Fig. 1). Fluid inclusions that are trapped at *PT* conditions within the single-phase vapor field (e.g., at point "3" in Fig. 1) have a relatively low density (less than the critical density of 0.443 g/cm^3).

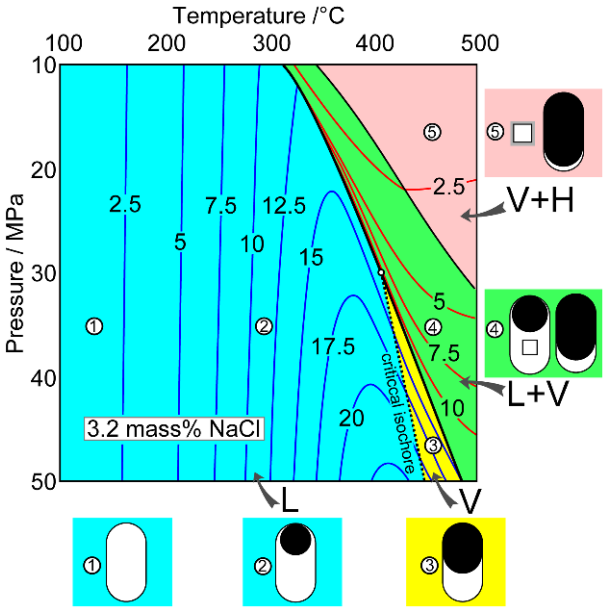

Figure 1. Phase equilibria, quartz solubility isopleths and fluid inclusion types as a function of temperature and pressure for fluid of seawater salinity (3.2 mass% NaCl). The liquid-vapor curve is shown by the thick black line; the critical point is shown by the open circle; the liquid-vapor-halite curve is shown by the thin black line; and the critical isochore is shown by the dashed line. The blue curves are quartz solubility isopleths in the single-phase field in mmolal. The red curves are bulk quartz solubility isopleths in the liquid+vapor and vapor+halite fields, with the bulk salinity maintained at 3.2 mass% NaCl. H_2O-NaCl phase equilibria are determined using the model of [12] and quartz solubility is determined using the model of [13]. The panels along the bottom and right-hand side show the room-temperature phase ratios of fluid inclusions trapped at points 1 to 5 (the inclusions are approximated as cylinders with hemispherical ends).

These inclusions contain > 60 volume percent vapor at room temperature and homogenize to the vapor phase by expansion of the vapor phase to fill the inclusion at the homogenization temperature.

To the high temperature side of the liquid-vapor curve, fluid inclusions trapped in the liquid + vapor field are represented by fluid inclusion assemblages containing coexisting liquid-rich and vapor-rich inclusions (e.g., point "4" in Fig. 1). When heated, the liquid-rich inclusions homogenize by shrinkage and disappearance of the vapor bubble, and the vapor-rich inclusions homogenize by expansion of the vapor bubble to fill the inclusion. Both the liquid-rich and the vapor-rich inclusions homogenize at the same temperature, which is equal to the trapping temperature. Throughout most of the *PT* range in the liquid + vapor field shown in Fig. 1, the salinity of the liquid phase is sufficiently high (> 26.2 mass% NaCl) such that the liquid-rich inclusions will contain a halite daughter mineral in addition to halite-saturated liquid and vapor at

room temperature. Meanwhile, the coexisting vapor-rich inclusions will have salinities less than 3.2 mass% NaCl, and contain a relatively large vapor bubble (> 60 volume percent of the inclusion). Because the liquid salinity throughout most of the two-phase region is significantly greater than the salinity of seawater, whereas the vapor salinity is less than, but close to, that of seawater, a much larger proportion of vapor will be generated during phase separation, and the system is therefore vapor-dominated. In other words, the mass (and volume) fraction of vapor is significantly greater than the fraction of liquid, throughout most of the liquid + vapor field.

At moderately high temperatures and low pressures, vapor + halite is the stable phase assemblage. Fluid inclusions that trap the vapor phase in this field would have a low salinity (~0 mass% NaCl through the *PT* range shown in Fig. 1) and low density (e.g., point "5" in Fig. 1) and would appear to be filled with only vapor (i.e., no liquid would be visible) at room temperature. Halite mineral inclusions might coexist with the vapor-rich inclusions in the fluid inclusion assemblage (Fig. 1), although such liquid-absent inclusions would be difficult to recognize petrographically because quartz and halite have similar indices of refraction (1.544).

The foregoing discussion describes room temperature characteristics of fluid inclusions trapped at various *PT* conditions, assuming that fluid inclusions are, indeed, trapped at those conditions. A related question is whether we would expect fluid inclusions to be trapped at any particular point within a hydrothermal system. In this study, we assume that fluid inclusions (especially primary fluid inclusions) are only trapped when quartz is being precipitated (see, for example, Fig. 2-1 in [9]). We recognize, however, that fluid inclusions may also be trapped as a result of dissolution-precipitation processes associated with crack healing. Dissolution-precipitation and crack healing can occur without any change in quartz solubility, as a result of the higher surface free energy of irregular grains and fracture surfaces. Thus, silica can be redistributed to minimize surface area by healing cracks, even if the *PT* conditions and bulk quartz solubility are not changing. This process is responsible for the formation of secondary and pseudosecondary inclusions, and it is the process by which synthetic fluid inclusions are prepared in laboratory experiments [16]. In the present study we consider the formation of primary fluid inclusions that are trapped in response to hydrothermal circulation. In hydrothermal systems, primary fluid inclusions are trapped during mineral growth when quartz-saturated fluid experiences a decrease in quartz solubility, owing to changes in temperature, pressure and/or composition. Whether quartz dissolution or precipitation should be expected as a result of changing *PTX* conditions during fluid flow may be predicted using the quartz-solubility isopleths contoured on Fig. 1 (blue curves). For example, at temperatures below about 300°C, quartz solubility in a 3.2 mass% NaCl fluid is mostly insensitive to pressure, and quartz solubility increases with increasing temperature (Fig. 1). Therefore, quartz may precipitate in response to decreasing temperature, regardless of the pressure, at temperatures below ~300°C.

At temperatures above ~300°C and pressures above ~20 MPa, quartz solubility reaches a local isobaric maximum, and begins to decrease with increasing temperature – a phenomenon referred to as retrograde solubility (Fig. 1). Retrograde solubility occurs in the vicinity of the critical isochore because the fluid density is sensitive to small changes in temperature and decreases significantly as temperature increases [17]. Thus, within this *PT* region increasing temperature tends to greatly reduce the number of water molecules per unit volume available to solvate the dissolved silica species [17, 18]. Therefore, the relatively sharp decrease in fluid density within a few tens of degrees Celsius of the critical isochore results in a decrease in quartz solubility with increasing temperature (Fig. 1). Within this range of pressure-temperature conditions, quartz precipitation is promoted by increasing temperature within the *PT* region of retrograde solubility. In addition, quartz solubility in the retrograde region decreases with decreasing pressure (Fig. 1), such that precipitation is also promoted by pressure decrease.

In the two-phase liquid + vapor region shown on Fig. 1, quartz solubility in the liquid phase is relatively higher, and quartz solubility in the vapor phase is relatively lower, compared to quartz solubility in the immediately adjacent single-phase region. The bulk quartz solubility in the liquid + vapor depends on the mass proportions of liquid and vapor present. In Fig. 1, the bulk quartz solubility is shown for a bulk salinity of 3.2 mass% NaCl based on mass-balanced liquid and vapor proportions (Fig. 1, red curves). Because the liquid salinity in the liquid + vapor field is greater than 30 mass% NaCl throughout most of the *PT* conditions shown in Fig. 1, a composition of 3.2 mass% NaCl requires a large proportion of vapor and relatively little liquid to satisfy the bulk composition (as described above). Therefore, the bulk quartz solubility in the two-phase field is dominated by the solubility of quartz in the vapor. Thus, as temperature is increased within the single-phase field and the temperature of the liquid-vapor curve is reached, quartz solubility decreases at the single-phase to two-phase interface. Furthermore, if a single-phase fluid of a fixed composition is heated such that immiscibility occurs, and the bulk salinity of the two-phase immiscible fluid pair remains the same as

the initial salinity before immiscibility, the solubility of quartz will decrease sharply upon crossing from the one-phase into the two-phase field. The change in solubility with temperature across the interface is significantly greater than the rate of solubility change with temperature anywhere within the single-phase field (Fig. 1). Thus, quartz may precipitate as a fluid is heated and undergoes liquid-vapor immiscibility. The gradient of quartz solubility (change in solubility as a function of temperature) across the liquid-vapor curve is steeper than the gradients within the single-phase field, making phase separation an important process leading to quartz precipitation in the vicinity of the liquid-vapor curve [19]

2. Methods

In this study we describe the variation in room temperature phase relationships and microthermometric characteristics of fluid inclusions trapped at various locations within a generic sub-seafloor hydrothermal system. The petrographic and microthermometric characteristics of the fluid inclusions are interpreted in terms of processes occurring in the sub-seafloor environment, and we consider how these processes affect the solubility of quartz. We model hydrothermal circulation using the code *FISHES* [20] which solves the conservation equations governing multi-component, multi-phase fluid flow in porous media. Details of the fluid-flow modeling procedures are fully described in [21, 22] and details of quartz precipitation and dissolution systematics in the sub-seafloor are described in [23].

We model hydrothermal convection within a 1.5 km-wide by 1 km-deep cross-section perpendicular to the ridge axis (Fig. 2). The cross-section approximates one-half of the complete hydrothermal system, with an identical cross-section (not shown) mirrored on the left side of the ridge axis. The top boundary represents the seafloor, and is set to a constant pressure of 25 MPa (representing cold hydrostatic pressure approximating 2.5 km of seawater). The lower left corner represents the top of the conductive boundary layer above the center of the axial magma chamber. To simulate the top of the conductive boundary layer, the bottom boundary is set to a constant temperature of 450°C for a distance of 500 m from the ridge axis; from this point to the right hand side of the cross section temperature decreases linearly to 300°C (Fig. 2). Keeping the bottom temperature constant assumes a constant input of new magma (and heat) from below.

The cross-section is divided into 40 by 60 square boxes, or cells. The permeability is assumed to be homogeneous and constant at 10^{-13} m^2, although we recognize

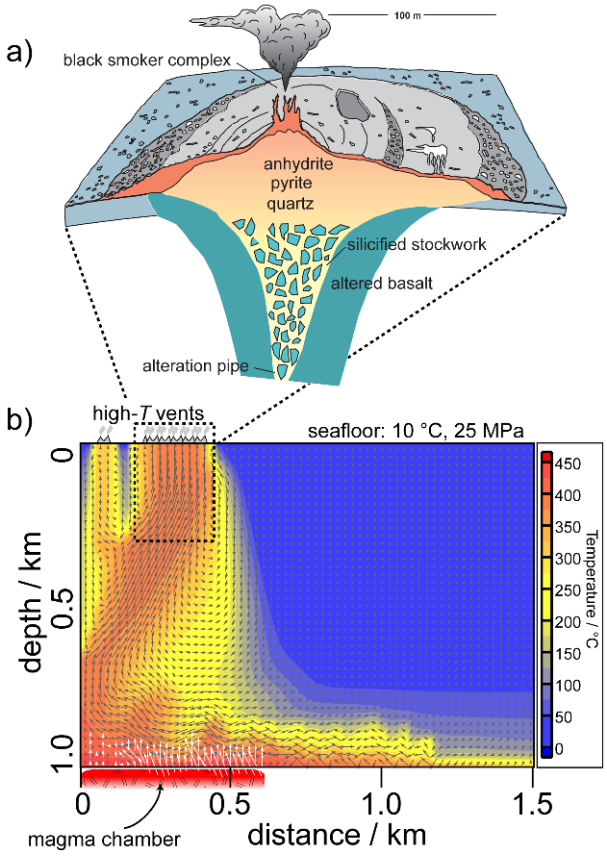

Figure 2. **(a)** Schematic cross-section of a VMS-forming hydrothermal system, modified from [4]. **(b)** A two-dimensional fluid-flow simulation of a mid-ocean ridge-crest hydrothermal system after 80 years of simulated time, with the dashed box showing the approximate location of the stockwork and seafloor vent from **(a)**. The *x* and *y* axes are the distance from the ridge axis and the depth below seafloor, respectively, and the simulation represents a 2-D slice perpendicular to the strike of the ridge. Fluid temperature is contoured, and overlain by the fluid flow vectors of liquid (gray) and vapor (white). The axial magma chamber (the heat source) resides under the left-hand side. Cold seawater enters the seafloor on the upper right-hand side, flows downward with little temperature change and then is heated as it flows along the bottom from right to left. Near the ridge axis and above the heat source (left side) the fluid rises as hot fluid plumes to produce high-temperature vents at the seafloor on the upper left-hand side.

that as quartz dissolves or precipitates that the permeability of the system will change. The right, left and bottom boundaries are impermeable to fluid flow, whereas the top boundary allows fluid flux into and out of the system. With this geometry and these boundary conditions, cold seawater enters the sub-seafloor at the upper right-hand side, flows downward into the subsurface, is heated as it flows from right to left along the bottom, and finally rises along the left-hand side (near the ridge axis) to vent at the seafloor at the upper left (Fig. 2). The temperature dis-

tribution and the flow pattern after 80 years of simulated time are shown in Figure 2. At this time in the evolution of the system, seawater undergoes phase separation (boiling) to produce high-salinity brine and low-salinity vapor (illustrated by the white arrows on the lower left of Fig. 2) immediately above the axial magma chamber, where *PT* conditions are within the liquid + vapor field (Fig. 1).

The two-dimensional flow model employed here accounts for fluid flow at every cell interface, and at every time step. As such, mixing of hydrothermal fluids with cold ambient seawater is implicitly included in the simulations. Fluid mixing is commonly inferred from VMS FI and vent fluid chemistry [3, 10], and our model allows us to consider the effects of fluid mixing on fluid phase equilibria and quartz solubility in the submarine hydrothermal environment.

We calculate quartz solubility in H_2O-NaCl fluids (representing seawater and immiscible brine and vapor) using the model of [13]. Quartz dissolves when the quartz solubility in the fluid increases along its flow path, and quartz precipitates in the opposite scenario. The details of the quartz dissolution and precipitation modeling are described in [23]. We monitor the solubility of quartz in each aliquot of fluid traversing an interface between two adjacent cells (i.e., fluid flowing from one cell into the adjacent cell). If the aliquot becomes quartz-supersaturated in the process, then the fluid precipitates quartz in the cell it is entering such that equilibrium is maintained. Conversely, if the fluid becomes quartz-undersaturated as it crosses the interface, then it dissolves quartz in the cell it is entering to maintain equilibrium. Thus, the amount of quartz dissolution and precipitation that occurs at each point depends on the quartz solubility gradient across the adjacent cells and the rate of fluid mass flux between those cells [19, 23].

In the present study we do not specify a lithology for the oceanic lithosphere through which fluids are flowing, and we assume that the fluid is in equilibrium with quartz throughout the system. We recognize, however, that in the host rocks of some VMS-type deposits (particularly the Cyprus-type ophiolitic basalt-hosted variety), quartz is absent from the unaltered mineral assemblage. Our assumption of quartz saturation is partly based on the observation that seawater rapidly achieves a dissolved silica content consistent with the solubility of quartz when it is reacted with unaltered basalt at 300-500°C [24, 25]. Silica is dissolved by interaction of heated seawater with silicate minerals and especially basaltic glass, and the activity of silica in solution increases until equilibrium with quartz is achieved.

To predict the distribution of fluid-inclusion petrographic and microthermometric characteristics within the fluid-flow model, we record the fluid pressure, temperature, salinity and density in each cell. The fluid density and salinity are calculated by the *FISHES* package [20] using lookup-tables based on the equation of state of [26]. The validity of the lookup-table interpolation method employed by *FISHES* has been tested and shown to represent the known phase equilibria and volumetric properties of H_2O-NaCl fluids with acceptable accuracy [20]. The fluid densities and salinities at the *PT* conditions of each cell, determined by *FISHES* [20], are used in the subsequent calculations of FI properties, as described below.

The temperature of melting of the last solid in the inclusion to disappear (either ice, hydrohalite or halite, depending on whether the fluid has salinity less than 23.2 mass% NaCl, between 23.2-26.2 mass% NaCl or greater than 26.2 mass% NaCl, respectively) was estimated using the equations of [27, 28]. Those equations, which express the salinity as a function of melting temperature, cannot be rearranged to solve for last melting temperature as a function of salinity, thus the last melting temperature was determined by iteration, using a halving technique.

The homogenization temperature of inclusions was estimated using the *PT* location of the liquid-vapor curves from the model of [29] and the isochore dP/dT slopes from the model of [30]. The homogenization temperature is found by identifying the homogenization temperature for the given fluid salinity that yields an isochore (from [30]) that passes through the *P* and *T* of fluid inclusion formation predicted by the fluid flow model. An alternative procedure to estimate homogenization temperature involves computing the vapor-saturated fluid density using the model of [31], and determining the temperature at which the vapor-saturated fluid density equals the known fluid density at the formation conditions. These two alternative methods to estimate homogenization temperature yielded identical results within the precision of the data. Similar to the method described above to determine the last melting temperature, all iterative calculations were solved using a halving technique.

For cells containing both liquid and vapor (zones of immiscibility or boiling), the properties of liquid-rich and vapor-rich inclusions were calculated assuming that each inclusion type trapped only a single phase, either liquid or vapor. The temperature of melting of the last solid in these inclusions was determined using the same methods as described above. It was not necessary to determine the homogenization temperatures of these inclusions because, for inclusions trapped at vapor-saturated conditions, i.e., in the two-phase field, the homogenization temperature equals the trapping temperature [32].

Inclusions with nominal homogenization temperature less

than 100°C are assumed to remain metastable during cooling from trapping conditions to room temperature and remain as single-phase, liquid-filled inclusions. Aqueous fluid inclusions with densities such that the homogenization temperature should be < ~100°C rarely nucleate a bubble during cooling [9, 15].

The room-temperature phase ratios of the inclusions were calculated by mass balance, assuming a vapor density of zero g/cm^3, halite density of 2.17 g/cm^3 and salinity-dependent liquid density calculated using the model of [31]. The volume and area proportions of the phases at room temperature were computed assuming cylindrical inclusions with hemispherical ends, spherical vapor bubbles (unless the radius exceeded the radius of the cylindrical inclusion, in which case the bubble was also cylindrical with hemispherical ends), and cubic halite crystals [33, 34].

3. Results

Figure 3 shows the distribution of areas in which quartz dissolution and precipitation occur after 80 years of simulated time. While Figure 3 shows where quartz is being dissolved and where it is being precipitated, the fluid *PTX* gradients responsible for dissolution-precipitation vary between different locations in the system. Quartz precipitation occurs in some cases as a result of cooling, in other cases as a result of heating, and in yet other cases as a result of phase separation, in different areas of the cross-section. Along the bottom of the cross section, from approximately 0.5 to 1.0 km from the ridge axis, quartz precipitates (Fig. 3) as the fluid flows from right to left and is heated through the retrograde quartz solubility range (see Fig. 1). In this region, quartz precipitates as a result of decreasing quartz solubility with increasing temperature, i.e., retrograde solubility. Along the bottom of the cross section at distances up to approximately 0.5 km from the ridge axis (Fig. 3), quartz precipitates as the fluid temperature is increased and intersects the liquid-vapor curve (see Fig. 1). In this part of the system, quartz precipitation is a result of the relatively large decrease in quartz solubility that occurs as the fluid crosses from the single-phase region into two-phase liquid + vapor region, with relatively little change in temperature. Within the plume that rises from depth to the seafloor near the ridge axis (relatively high temperature region shown on the left side of Fig. 2), quartz precipitates in response to decreasing pressure, combined with a slight temperature decrease. In several localized zones near the bottom of the system, quartz precipitates as small fluid plumes ascend and quartz dissolves as fluid condenses and descends. These zones of dissolution and precipitation vary over short distances as the fluid flows along the bottom

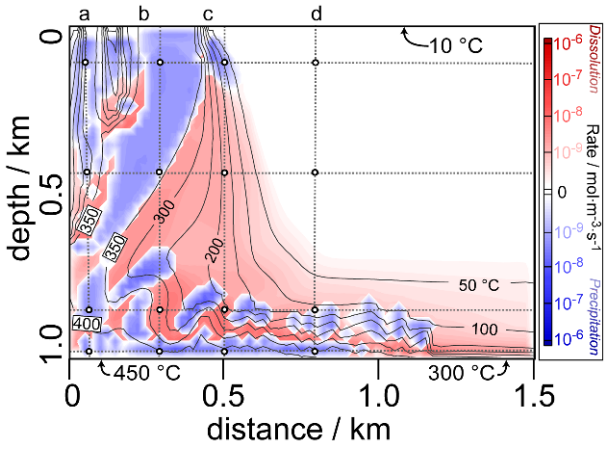

Figure 3. Distribution of regions of quartz dissolution and precipitation for the same time step shown on Figure 2. Dissolution rate is contoured in red, and precipitation rate is contoured in blue. Thin solid lines show the fluid temperature contours, and the white circles at the intersections of dashed lines show the locations in the system where characteristics of fluid inclusion have been determined and are shown on Figure 4.

from right to left (small zones of precipitation separated by regions of dissolution from about 1.25 to 0.25 km, Fig. 3). A similar distribution of zones of precipitation and dissolution has been described previously in [23].

Characteristics of fluid inclusions that would be trapped at selected points on the cross section shown in Fig. 3 (the white circles on the dashed-line grid) are shown on Fig. 4. In the deepest part of the system (1000 m), vapor-rich inclusions (FI that homogenize to the vapor phase) are trapped at the greatest distance from the ridge axis (column "d", 1000 m depth on Fig. 4) as the fluid flows from right to left and is heated as it approaches the magmatic heat source. These inclusions are trapped as a result of the retrograde quartz solubility in this region that leads to quartz precipitation as the fluid is heated. In the submarine *PTX* range examined here, vapor-rich inclusions (without coexisting liquid-rich inclusions in the same assemblage) are unequivocal evidence of trapping in the retrograde quartz solubility field, although liquid-rich inclusions may also be trapped in the retrograde region at lower temperature (Fig. 1). Fluid inclusions trapped at the same distance from the ridge axis but at slightly shallower depths have significantly higher density and lower T_h, owing to the steep thermal gradient above the conductive boundary layer (column "d", 900 m depth on Fig. 4).

As the deep fluid continues to flow towards the ridge axis, it enters the two-phase liquid + vapor region, and coexisting liquid-rich and vapor-rich inclusions are trapped (columns "a", "b" and "c" at 1000 m depth on Fig. 4). Above the two-phase zone, along the rising plume, fluid inclusions are liquid-rich with salinity slightly higher than

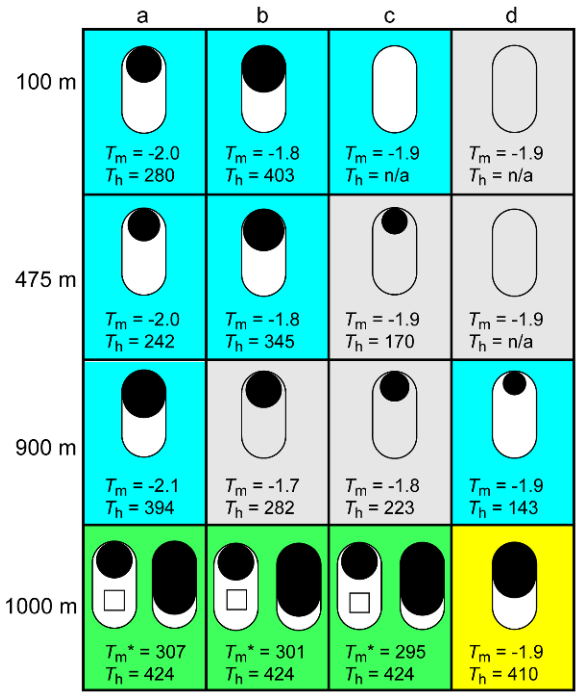

Figure 4. Fluid inclusion characteristics at the locations within the hydrothermal system shown on Figure 4. The background color of each panel corresponds to the phase field in which the FI were trapped (refer to Figure 1 for color code).The panels with gray background indicate that fluid inclusions are not trapped at these conditions because quartz is not precipitated and/or is being dissolved at that location - the characteristics of the fluid inclusions that would be trapped (perhaps along healed fractures in quartz or in minerals other than quartz) are shown. Room-temperature phase ratios are determined assuming a cylindrical FI with hemispherical ends. All temperatures are in degrees Celsius. T_h refers to liquid-vapor homogenization temperature; T_m refers to ice melting temperature; T_m* refers to halite melting temperature for the liquid-rich inclusions in the liquid + vapor field, and all vapor-rich inclusions in the liquid + vapor field have ice melting temperatures of -0.1°C.

or lower than that of seawater, and have homogenization temperatures between 200 and 400°C (column "b", 100 m and 475 m depth; and column "a", 100, 475 and 900 m depth, Fig. 4). To either side of the plume nearby, homogenization temperatures are significantly lower and vapor-absent inclusions may occur, owing to mixing with cold ambient seawater.

4. Discussion

4.1. Qualitative assessment of effects of varying boundary conditions

The present study assumed a homogeneous permeability of 10^{-13} m^2. If permeability were higher or lower, then mass flux rates would be correspondingly higher or lower, respectively. Extensive fluid-flow modeling of the system described here, using a range of permeabilities from 10^{-14} m^2 to 10^{-12} m^2, shows that flow patterns are generally unaffected by varying the permeability within this range (in a homogeneous permeability cross-section) [21, 22]. The main effects of varying permeability are to change the timescale required to reach quasi-steady state, and the magnitude of mass flux [21, 22]. Thus, in a higher permeability system than the one described here, quartz precipitation and fluid inclusion trapping would occur at approximately the same locations as described above, and the fluid inclusions would have the same microthermometric and phase characteristics, but the amount of quartz precipitated in a given amount of time would be greater.

We may consider in a qualitative sense the effect that quartz precipitation would have on the permeability distribution. For example, in the stockwork zone of the JADE hydrothermal field, fractures are commonly self-sealed by quartz and silica precipitation [3]. If permeability evolution were incorporated into the present model, regions in which quartz is being precipitated would undergo a decrease in permeability. Similarly, quartz dissolution would tend to increase permeability over time. These changes in permeability may significantly affect hydrothermal convection, thus shifting the locations where particular fluid *PVTX* conditions occur in the hydrothermal system. Moreover, the system may not achieve a pseudo-steady state, as does the constant permeability system described here. Concomitantly, the properties of fluid inclusions, and their spatial distribution in the system, would vary with time. A comprehensive assessment of the temporal variability of FI properties in a system with evolving permeability is beyond the scope of the present study, but a future study is planned to investigate these effects.

In the present study the maximum bottom temperature was 450°C. Numerical simulations have shown that fluid flow patterns are relatively insensitive to the bottom boundary temperature [21, 22]. However, we may qualitatively assess the effect of varying the maximum bottom temperature on the types and distribution of fluid inclusions that will be trapped in the hydrothermal system. If the bottom temperature is reduced to less than 450°C, the liquid salinity in the two-phase region would be reduced. For example, at 425°C the liquid salinity would be ~15 mass% NaCl (assuming the same depth), compared to ~40 mass% NaCl in the liquid phase at 450°C. At lower temperature and, concomitantly lower liquid salinity, the liquid-rich fluid inclusions would not be halite saturated at room temperature. These inclusions would still be recognizable as representing a trapped immiscible brine phase because

they would have relatively low ice-melting temperatures of -11.8°C (significantly lower than the ice-melting temperature of seawater of (~-1.9°C) and would likely coexist with vapor-rich inclusions in the same fluid inclusion assemblage. If the maximum bottom temperature is reduced further, for example to 400°C, then phase separation would not occur, assuming that the seawater depth and pressure at the seafloor remains the same. In that case, the high-temperature region below the plume and near the ridge axis would lie approximately along the isobaric quartz solubility minimum, and little or no precipitation of quartz would result [23]. The absence of phase separation in the system would be evidenced by examination of fluid inclusions in the stockwork zone as well, because all inclusions in the fluid inclusion assemblage would have similar room temperature phase ratios and all would have the salinity of seawater, and thus have ice-melting temperatures of -1.9°C.

The results presented here are *sensu stricto* applicable to submarine hydrothermal systems, but we may also consider how these results relate to other (continental) magmatic-hydrothermal systems. In the present model the circulating fluid is seawater with initial salinity of 3.2 mass% NaCl, whereas in continental magmatic-hydrothermal systems the fluid may have a wide range in composition and be derived from a variety of other sources (meteoric, magmatic and/or connate [35]). The *PT* conditions that define the liquid, vapor, and two-phase liquid + vapor fields are composition dependent [34, 36]. Additionally, the model described here assumes an upper boundary pressure of 25 MPa, representing an overlying seawater depth of 2500 m, whereas subaerial hydrothermal systems have an upper surface pressure of 0.1 MPa. Because of the relatively low surface pressure associated with subaerial hydrothermal systems, when phase separation occurs in the subsurface it commonly continues as the fluids ascend all the way to the surface [19]. This is in contrast with the results of the present model, in which fluid phase immiscibility is limited to the lowermost region of hydrothermal convection, and boiling stops as the fluid migrates upward to the seafloor.

4.2. Distribution of fluid inclusion characteristics in VMS deposits

Volcanogenic massive sulfide deposits form at or near the seafloor, typically associated with lenses or mounds near seafloor vents (Fig. 2) and with a stockwork zone at depths up to several hundred meters below the vents [1, 4]. As such, the fluid inclusion types on Fig. 4 that are most likely to be found in VMS stockworks are those shown in columns "a" and "b" at 100 m and 475 m. These inclusions are liquid-rich and contain vapor bubbles occupying about 35 to 50 volume percent of the inclusion, and they homogenize to the liquid phase at 200 to 400°C. Low-temperature microthermometry of these inclusions would reveal variable salinities slightly higher or lower than that of seawater as a result of trapping mixtures of vapor, coexisting brine and entrained seawater. These results are consistent with fluid-inclusion studies of Kuroko VMS deposits [5] and their modern analogues [3], in which ore-forming fluids have variable salinities, ranging from 3.5 to 5 mass% NaCl. These salinities reflect mixing between seawater (3.2 mass% NaCl) and phase-separated brine and/or vapor from the deeper part of the system (Fig. 2). Notice that, although the vapor phase generated during phase separation is less dense than the coexisting brine, the brine is not entirely sequestered at the base of hydrothermal convection, as reported by [37]. Rather, some of the brine may be entrained into the rising hydrothermal fluid, leading to vent fluid salinities that are sometimes less than and sometimes greater than that of seawater [20–22]. When phase separation occurs at the base of the hydrothermal convection system, base metals are preferentially concentrated into the brine, such that fluid inclusions in sulfide minerals are always more saline than fluid inclusions in other hosts at the JADE hydrothermal field [3]. Thus, it appears that phase separation influences sulfide mineralization in VMS deposits, even though phase separation occurs deep beneath the mineralized zone.

In the model presented here, quartz mainly precipitates as a result of three separate but related processes: as a result of heating as the fluid flows through the retrograde solubility region near the base of the hydrothermal system; as a result of boiling or immiscibility as the fluid enters the liquid-vapor region of *PT* space; and during decompression as the fluid ascends in the plume to vent at the seafloor. Fluid inclusions trapped within the retrograde quartz-solubility region are represented on column "d" at 1000 m depth on Fig. 4. These fluid inclusions have seawater salinity (ice-melting temperature of -1.9°C) and homogenize to the vapor phase or by critical behavior. Fluid inclusions trapped in the liquid-vapor immiscibility region are shown on columns "a", "b" and "c" at 1000 m depth on Fig. 4. Fluid inclusion assemblages trapped in this part of the hydrothermal system would contain coexisting halite-bearing liquid-rich inclusions and low-salinity vapor-rich inclusions. Inclusions trapped within the prograde solubility region are represented by columns "a", "b" and "c" at 100 m depth; "a" and "b" at 475 m depth; and "a" at 900 m depth on Fig. 4. These inclusions have salinities slightly greater or less than that of seawater and homogenize to the liquid phase by vapor bubble disappearance. In this environment, if a

growth zone or fluid inclusion assemblage in quartz consists of only liquid-rich inclusions, then that quartz likely precipitated as a result of cooling through the prograde solubility region (Fig. 1). Likewise, if the inclusions in one growth zone are all vapor-rich, then that growth zone likely formed as a result of heating (or pressure decrease) within the retrograde solubility region (Fig. 1). Fluid inclusion assemblages containing coexisting liquid-rich and vapor-rich inclusions indicate that the quartz host precipitated in response to fluid phase immiscibility. These fluid inclusion properties, obtained from petrography and/or microthermometry, can be used to interpret thermal and fluid processes associated with quartz vein formation.

Fluid inclusion types shown on Fig. 4, together with their spatial variation, can be used to infer where a sample formed within the overall sub-seafloor hydrothermal system relative to where VMS-type mineralization would be expected to occur. Thus, the distribution of fluid inclusion types provides vectors towards possible stockwork mineralization. If erosion and uplift across the system (from the ridge axis outward) have been uniform, or if samples are obtained from a single depth horizon within the system through drilling, homogenization temperatures of the inclusions will increase in the direction towards stockwork mineralization. For example, at a depth of 100 m (Fig. 4), if fluid inclusions were sampled at the locations represented by columns "a", "b" and "c" then the inclusions at columns "a" and "b" would be the best indicators of potential stockwork mineralization, where homogenization temperatures are 280°C at column "a" and ~400°C at column "b" at 100 m depth (Fig. 4). This interpretation is based on the observation that fluid inclusion temperatures in VMS stockworks are typically in the range 200-400°C [3, 4], and the only part of the system modeled here that shows those temperatures in the upflow zone is associated with the plume in the vicinity of columns "a" and "b".

If a sample collected during an exploration program contains coexisting liquid-rich and vapor-rich inclusions, the sample likely formed at the base of the hydrothermal convection system, and the mineralized stockwork (if present) is above the sample location (columns "a", "b" and "c" at 1000 m on Fig. 4). If the sample was collected from a surface outcrop, the mineralized zone has likely been destroyed and removed by erosion, and the location would thus not represent a high-priority target. If the sample came from a drill core and if the ore zone was not intersected before reaching this sample depth, the ore zone (if it exists) is likely offset laterally from the drill hole trajectory.

If samples contain assemblages with only vapor-rich inclusions with relatively high homogenization temperatures, the samples likely originated at the periphery of the system and at depths greater than the depth of mineralization (column "d" at 1000 m on Fig. 4). In this case, areas both lateral to and at shallower depths should be explored. As noted above, however, if the sample came from a surface outcrop, any mineralization that might have existed has likely been removed by erosion.

In addition, if following mineralization the deposit has been tilted and/or deformed, the spatial distribution of inclusion types may help to identify the up direction (and direction towards the stockwork) in the volcanic pile.

The periphery of the submarine hydrothermal system that is unlikely to host VMS mineralization is characterized by the absence of quartz mineralization (thus the absence of quartz-hosted primary fluid inclusions; e.g. the locations indicated by the gray background on Fig. 4).

While the specific petrographic and microthermometric features described above are characteristic of various parts of the submarine hydrothermal system, it is highly unlikely that one would be able to predict where in the system a sample came from by looking at a single sample. The use of fluid inclusions in mineral exploration is based on the fact that in some types of deposits, such as epithermal precious metals deposits [33, 38] and porphyry copper deposits [39, 40], fluid inclusions show systematic variations in petrographic and microthermometric behavior as a function of location relative to mineralization. Thus, several samples must be examined to identify trends in fluid inclusion characteristics that define vectors to guide the explorationist toward potential mineralization.

5. Summary

Fluid inclusions trapped in quartz in subseafloor hydrothermal systems record the physical and chemical properties of fluids from which quartz precipitated. Areas (and *PT* conditions) where quartz precipitation does not occur or where quartz dissolution occurs are likely to be under-represented in the primary fluid inclusion record in this environment. The characteristics of fluid inclusions and the spatial distribution of fluid-inclusion types within the area affected by hydrothermal convection can be used to infer where a sample is located relative to the relatively smaller stockwork region, allowing the use of fluid inclusions to provide "vectors" towards potential VMS-type mineralization. Liquid-rich inclusions with 35-50 volume percent vapor, homogenization temperatures from 200-400°C and salinity slightly lower or higher than seawater are most closely associated spatially with the zone where massive sulfide ore would be found if it exists. Lower homogenization temperatures occur adjacent to the stockwork. Vapor-rich inclusions, with or without coexist-

ing liquid-rich inclusions, occur beneath the stockwork at the deepest levels of circulation.

Acknowledgements

The authors thank two anonymous reviewers for comments that greatly improved the manuscript. We thank Kayla Lewis for help with the *FISHES* code used to model fluid flow. We also thank Miriam Baumgartner and Ronald Bakker for their editorial efforts. Financial support for MS-M was provided by the Institute for Critical Technology and Applied Science (ICTAS) at Virginia Tech. Financial support for LH was provided by the US National Science Foundation under grant no. OCE-0819084 to RPL. This material is based upon work supported by the US National Science Foundation under grant no. OCE-0928472 to RJB, RPL and JDR.

References

[1] Galley A.G., Hannington M., Jonasson I., Volcanogenic massive sulphide deposits. In: W.D. Goodfellow (Ed.), Mineral Deposits of Canada: A Synthesis of Major Deposit-types, District Metallogeny, the Evolution of Geological Provinces, and Exploration Methods. Geological Association of Canada, St. John's NL, 2007, 141-161

[2] Vanko D.A., Bach W., Roberts S., Yeats C.J., Scott S.D., Fluid inclusion evidence for subsurface phase separation and variable fluid mixing regimes beneath the deep-sea PACMANUS hydrothermal field, Manus Basin back arc rift, Papua New Guinea. *J. Geophys. Res.*, 2004, 109, B03201

[3] Lüders V., Pracejus B., Halbach P., Fluid inclusion and sulfur isotope studies in probable modern analogue Kuroko-type ores from the JADE hydrothermal field (central Okinawa Trough, Japan). *Chem. Geol.*, 2001, 173, 45-58

[4] Hannington, M.D., Galley, A.G., Herzig, P.M., Petersen, S., Comparison of the TAG mound and stockwork complex with Cyprus-type massive sulfide deposits. In: P.M. Herzig, S.E. Humphris, D.J. Miller, and R.A. Zierenberg (Eds.), Proceedings of the ocean drilling program, scientific results volume 158. Integrated Ocean Drilling Program, College Station TX USA, 1998, 389-415

[5] Pisutha-Arnond V., Ohmoto H., Thermal history, and chemical and isotopic compositions of the ore-forming fluids responsible for the Kuroko massive sulfide deposits in the Hokuroku District of Japan. *Econ. Geol. Mono.*, 1983, 5, 523-558

[6] Vanko D.A., Temperature, pressure, and composition of hydrothermal fluids, with their bearing on the magnitude of tectonic uplift at mid-ocean ridges, inferred from fluid inclusions in oceanic layer 3 rocks. *J. Geophys. Res.*, 1988, 93, 4595-4611

[7] Halbach, M., Halbach, P., Lüders, V., Sulfide-impregnated and pure silica precipitates of hydrothermal origin from the Central Indian Ocean. *Chem. Geol.*, 2002, 182, 357-375

[8] de Ronde C.E.J., Fluid chemistry and isotopic characteristics of seafloor hydrothermal system and associated VMS deposits; potential for magmatic contributions. In: J.F.H. Thompson (Ed.) Magmas, Fluids and Ore Deposits. Mineralogical Association of Canada, Ottawa ON Canada, 1995, 479-509

[9] Roedder E., Fluid Inclusions. Reviews in Mineralogy, 1984, 12, 644

[10] Von Damm K.L., Evolution of the hydrothermal system at East Pacific Rise 9°50'N; geochemical evidence for changes in the upper oceanic crust. *Geophys. Mono.*, 2004, 148, 285-304

[11] Nehlig, P., Salinity of oceanic hydrothermal fluids: a fluid inclusion study. *Earth Planet. Sci. Lett.*, 1991, 102, 310-325

[12] Driesner, T., Heinrich, C.A., The system H_2O-NaCl. Part I: Correlation formulae for phase relations in temperature-pressure-composition space from 0 to 1000°C, 0 to 5000 bar, and 0 to 1 XNaCl. *Geochim. Cosmochim. Acta*, 2207, 71, 4880-4901

[13] Akinfiev N.N., Diamond L.W., A simple predictive model of quartz solubility in water-salt-CO_2 systems at temperatures up to 1000°C and pressures up to 1000 MPa. *Geochim. Cosmochim. Acta*, 2009, 76, 1597-1608

[14] Knight, C.L., Bodnar, R.J., Synthetic fluid inclusions. IX. Critical PVTX properties of NaCl-H_2O solutions. *Geochim. Cosmochim. Acta*, 1989, 53, 3-8

[15] Roedder E., Metastable superheated ice in liquid-water inclusions under high negative pressure. *Science*, 1967, 155, 1413-1417

[16] Bodnar, R.J., Sterner, S.M., Synthetic fluid inclusions. In: G.C. Ulmer and H.L. Barnes (Eds.) Hydrothermal experimental techniques. Wiley-Interscience, New York NY USA, 1987, 423-457

[17] Kennedy, G.C., A portion of the system silica-water. *Econ. Geol.*, 1950, 45, 629-653

[18] Dolejš, D., Manning, C.E. Thermodynamic model for mineral solubility in aqueous fluids: theory, calibration and application to model fluid-flow systems. *Geofluids*, 2010, 10, 20-40

[19] Cline J.S., Bodnar R.J., Rimstidt J.D., Numerical simulation of fluid flow and silica transport and deposition

in boiling hydrothermal solutions; application to epithermal gold deposits. *J. Geophys. Res.*, 1992, 97, 9085-9103

[20] Lewis K.C., Lowell R.P., Numerical modeling of two-phase flow in the NaCl-H_2O system: Introduction of a numerical method and benchmarking. *J. Geophys. Res.*, 2009, 114, B05202

[21] Han L., Lowell R.P., Lewis K.C., The dynamics of two-phase hydrothermal systems at a seafloor pressure of 25 MPa: Application to EPR 9°50' N. *J. Geophys. Res.* (submitted for publication)

[22] Han, L., Exploring two-phase hydrothermal circulation at a seafloor pressure of 25 MPa: Application for EPR 9°50' N. MSc Thesis, Virginia Tech, Blacksburg VA USA, 2011

[23] Steele-MacInnis M., Han L., Lowell R.P., Rimstidt J.D., Bodnar R.J., The role of fluid phase immiscibility in quartz dissolution and precipitation in sub-seafloor hydrothermal systems. *Earth Planet. Sci. Lett.*, 2012, 321-322, 139-151

[24] Mottl, M.J., Holland, H.D., Chemical exchange during hydrothermal alteration of basalt by seawater. I: Experimental results for major and minor components of seawater. *Geochim. Cosmochim. Acta*,1978, 42, 1103-1115

[25] Seyfried, W.E., Bischoff, J.L., Experimental seawater-basalt interaction at 300°C, 500 bars, chemical exchange, secondary mineral formation and implications for the transport of heavy metals. *Geochim. Cosmochim. Acta*, 1981, 45, 135-147

[26] Anderko, A., Pitzer, K.S., Equation-of-state representation of phase equilibria and volumetric properties of the system NaCl-H_2O above 573 K. *Geochim. Cosmochim. Acta*, 1993, 57, 1657-1680

[27] Sterner S.M., Hall D.L., Bodnar R.J., Synthetic fluid inclusions. V. Solubility relations in the system NaCl-KCl-H_2O under vapor-saturated conditions. *Geochim. et Cosmochim. Acta*, 1988, 52, 989-1006

[28] Bodnar R.J., Revised equation and table for determining the freezing point depression of H_2O-NaCl solutions. *Geochim. Cosmochim. Acta*, 1993, 57, 683-684

[29] Atkinson Jr., A.B., A model for the PTX properties of H_2O-NaCl, MSc Thesis, Virginia Tech, Blacksburg VA USA, 2002

[30] Bodnar, R.J., Vityk, M.O., Interpretation of microthermometric data for H_2O-NaCl fluid inclusions. In: B. De Vivo and M.L. Frezotti (Eds.) Fluid inclusions in minerals, methods and applications. Virginia Tech, Blacksburg VA USA, 1994, 117-130

[31] Bodnar R.J., A method of calculating fluid inclusion volumes based on vapor bubble diameters and P-V-T-X properties of inclusion fluids. *Econ. Geol.*, 1983, 78, 538-542

[32] Roedder, E., Bodnar, R.J., Geologic pressure determinations from fluid inclusion studies. *Ann. Rev. Earth Planet. Sci.*, 1980, 8, 263-301

[33] Bodnar, R.J., Reynolds, T.J., Kuehn, C.A., Fluid inclusion systematics in epithermal systems. In: B.R. Berger and P.M. Bethke (Eds.) Reviews in Economic Geology, Geology and Geochemistry of Epithermal Systems. Society of Economic Geologists, Littleton CO USA, 1985, 73-98

[34] Bodnar, R.J., Introduction to aqueous-electrolyte fluid inclusions. In: I. Samson, A. Anderson and D. Marshall (Eds.) Fluid inclusions, analysis and interpretation. Mineralogical Association of Canada, Ottawa ON Canada, 2003, 81-100

[35] Kesler, S.E., Ore-forming fluids. *Elements*, 2005, 1, 13-18

[36] Bodnar, R.J., Burnham, C.W., Sterner, S.M., Synthetic fluid inclusions in natural quartz. III. Determination of phase equilibrium properties in the system H_2O-NaCl to 1000°C and 1500 bars. *Geochim. Cosmochim. Acta*, 1985, 49, 1861-1873

[37] Bischoff, J.L., Rosenbauer R.J., Salinity variations in submarine hydrothermal systems by layered double-diffusive convection. *J. Geol.*, 1989, 97, 613– 623

[38] Moncada, D., Mutchler, S., Nieto, A., Reynolds, T.J., Rimstidt, J.D., Bodnar, R.J., Mineral textures and fluid inclusion petrography of the epithermal Ag-Au deposits at Guanajuato, Mexico: Application to exploration. *J. Geochem. Explor.* (in press) DOI: 10.1016/j.gexplo.2011.12.001

[39] Bodnar, R.J., Fluid inclusion evidence for a magmatic source for metals in porphyry copper deposits. In: J.F.H. Thompson (Ed.) Magmas, fluids and ore deposits. Mineralogical Association of Canada, Ottawa ON Canada, 1995, 139-152

[40] Roedder, E., Bodnar, R.J., Fluid Inclusion Studies of Hydrothermal Ore Deposits. In: H.L. Barnes (Ed.) Geochemistry of hydrothermal ore deposits (3rd ed.). Wiley & Sons, Inc., New York NY USA, 1997, 657-698